

A Maximum Mass-to-Size Ratio in Scalar-Tensor Theories of Gravity

Tooru TSUCHIDA ^{*}, Go KAWAMURA [†] and Kazuya WATANABE [‡]
Department of Physics, Niigata University, Niigata 950-21, Japan.

Abstract

We derive a modified Buchdahl inequality for scalar-tensor theories of gravity. In general relativity, Buchdahl has shown that the maximum value of the mass-to-size ratio, $2M/R$, is $8/9$ for static and spherically symmetric stars under some physically reasonable assumptions. We formally apply Buchdahl's method to scalar-tensor theories and obtain theory-independent inequalities. After discussing the mass definition in scalar-tensor theories, these inequalities are related to a theory-dependent maximum mass-to-size ratio. We show that its value can exceed not only Buchdahl's limit, $8/9$, but also unity, which we call *the black hole limit*, in contrast to general relativity. Next, we numerically examine the validity of the assumptions made in deriving the inequalities and the applicability of our analytic results. We find that the assumptions are mostly satisfied and that the mass-to-size ratio exceeds both Buchdahl's limit and the black hole limit. However, we also find that this ratio never exceeds Buchdahl's limit when we impose the further condition, $\rho - 3p \geq 0$, on the density, ρ , and pressure, p , of the matter.

1 Introduction

Einstein's general relativity postulates that gravitational interactions are mediated by a tensor field, $g_{\mu\nu}$. It is also well-known that electro-magnetic interactions are mediated by a vector field, A_μ . One may therefore suspect that some unknown interactions may be mediated by scalar fields. Such theories have been suggested since before the appearance of general relativity. Moreover, it has been repeatedly pointed out over the years that unified theories that contain gravity as well as other interactions naturally give rise to scalar fields coupled to matter with gravitational strength. This motivation has led many theoretical physicists to study scalar-tensor theories of gravity (scalar-tensor theories) [1],[2],[3],[4]. The scalar-tensor theories are natural alternatives to general relativity, and gravity is mediated not only by a tensor field but also by a scalar field in these theories. Recently, such theories have been of interest as effective theories of string theory at low energy scales [5].

Many predictions of the scalar-tensor theories in strong gravitational fields are summarized in Ref.[4],[6],[7]. It has been found that a wide class of scalar-tensor theories can pass all experimental tests in weak gravitational fields. However, it has also been found that scalar-tensor theories exhibit different aspects of gravity in strong gravitational fields in contrast to

^{*}Electronic address:tsuchida@astro2.sc.niigata-u.ac.jp

[†]Electronic address:kawamura@astro2.sc.niigata-u.ac.jp

[‡]Electronic address:kazuya@astro2.sc.niigata-u.ac.jp

general relativity. It has been shown numerically that nonperturbative effects in the scalar-tensor theories increase the maximum mass of an isolated system such as a neutron star [6],[7].

In general relativity, the mass-to-size ratio of a star has physical significance, especially for an isolated system. Buchdahl has obtained a maximum value of the mass-to-size ratio of a static and spherically symmetric star under the following physically reasonable assumptions [8],[9],[10].

- No black hole exists.
- The constitution of the star is a perfect fluid.
- The density at any point in the star is a positive and monotonously decreasing function of the radius.
- An interior solution of the star smoothly matches an exterior solution, i.e., Schwarzschild's solution.

Buchdahl has obtained an upper limit of the mass-to-size ratio as $2M/R \leq 8/9$. We shall refer to this as the *Buchdahl inequality*.

Motivated by Buchdahl's theorem, we shall derive a modified Buchdahl inequality to obtain the maximum mass-to-size ratio in scalar-tensor theories. We then numerically examine the validity of the assumptions made in deriving the inequality. The applicability of our analytic results is also examined. This paper is organized as follows. In section 2, we summarize the basic equations in the scalar-tensor theories. In section 3, we derive a modified Buchdahl inequality in the scalar-tensor theories, and the numerical results are compared with the analytic results in section 4. A brief summary is given in section 5.

2 Basic equations

We shall consider the simplest scalar-tensor theory [1],[4],[11]. In this theory, gravitational interactions are mediated by a tensor field, $g_{\mu\nu}$, and a scalar field, ϕ . The action of the theory is

$$S = \frac{1}{16\pi} \int \sqrt{-g} \left[\phi R - \frac{\omega(\phi)}{\phi} g^{\mu\nu} \phi_{,\mu} \phi_{,\nu} \right] d^4x + S_{matter}[\Psi_m, g_{\mu\nu}], \quad (2.1)$$

where $\omega(\phi)$ is a dimensionless arbitrary function of ϕ , Ψ_m represents matter fields, and S_{matter} is the action of the matter fields. The scalar field, ϕ , plays the role of an effective gravitational constant as $G \sim 1/\phi$. Varying the action by the tensor field, $g_{\mu\nu}$, and the scalar field, ϕ , yields, respectively, the following field equations:

$$G_{\mu\nu} = \frac{8\pi}{\phi} T_{\mu\nu} + \frac{\omega(\phi)}{\phi^2} \left(\phi_{,\mu} \phi_{,\nu} - \frac{1}{2} g_{\mu\nu} g^{\alpha\beta} \phi_{,\alpha} \phi_{,\beta} \right) + \frac{1}{\phi} (\nabla_\mu \nabla_\nu \phi - g_{\mu\nu} \square \phi), \quad (2.2)$$

$$\square \phi = \frac{1}{3 + 2\omega(\phi)} \left(8\pi T - \frac{d\omega}{d\phi} g^{\alpha\beta} \phi_{,\alpha} \phi_{,\beta} \right). \quad (2.3)$$

Now we perform the conformal transformation,

$$g_{\mu\nu} = A^2(\varphi) g_{*\mu\nu}, \quad (2.4)$$

such that

$$G_* A^2(\varphi) = \frac{1}{\phi}, \quad (2.5)$$

where G_* is a bare gravitational constant, and we call $A(\varphi)$ a *coupling function*. Hereafter, the symbol, $*$, denotes quantities or derivatives associated with $g_{*\mu\nu}$. Then the action can be rewritten as

$$S = \frac{1}{16\pi G_*} \int \sqrt{-g_*} (R_* - 2g_*^{\mu\nu} \varphi_{,\mu} \varphi_{,\nu}) d^4x + S_{matter}[\Psi_m, A^2(\varphi)g_{*\mu\nu}], \quad (2.6)$$

where the scalar field, φ , is defined by

$$\alpha^2(\varphi) \equiv \left(\frac{d \ln A(\varphi)}{d\varphi} \right)^2 = \frac{1}{3 + 2\omega(\phi)}. \quad (2.7)$$

Varying the action by $g_{*\mu\nu}$ and φ yields, respectively,

$$G_{*\mu\nu} = 8\pi G_* T_{*\mu\nu} + 2 \left(\varphi_{,\mu} \varphi_{,\nu} - \frac{1}{2} g_{*\mu\nu} g_*^{\alpha\beta} \varphi_{,\alpha} \varphi_{,\beta} \right), \quad (2.8)$$

$$\square_* \varphi = -4\pi G_* \alpha(\varphi) T_*, \quad (2.9)$$

where $T_*^{\mu\nu}$ represents the energy-momentum tensor with respect to $g_{*\mu\nu}$ defined by

$$T_*^{\mu\nu} \equiv \frac{2}{\sqrt{-g_*}} \frac{\delta S_{matter}[\Psi_m, A^2(\varphi)g_{*\mu\nu}]}{\delta g_{*\mu\nu}} = A^6(\varphi) T^{\mu\nu}. \quad (2.10)$$

The conservation law for $T_*^{\mu\nu}$ is given by

$$\nabla_{*\nu} T_{*\mu}^{\nu} = \alpha(\varphi) T_* \nabla_{*\mu} \varphi. \quad (2.11)$$

The field equations (2.9) and (2.11) tell us that the *coupling strength*, $\alpha(\varphi)$, plays a role in mediating interactions between the scalar field, φ , and the matter. General relativity is characterized by having a vanishing coupling strength: $\alpha(\varphi) = 0$, i.e., $A(\varphi) = 1$. The Jordan-Fierz-Brans-Dicke theory is characterized by having a φ -independent coupling strength: $\alpha(\varphi) = \alpha_0 = \text{const.}$, i.e., $A(\varphi) = e^{\alpha_0 \varphi}$ [1],[6]. Observational constraints on the coupling strength are summarized in Appendix A.

3 Modified Buchdahl's theorem in scalar-tensor theories

In this section, we consider a static and spherically symmetric space-time with a perfect fluid. First, we derive a modified Buchdahl inequality. Then the inequality is reformulated to obtain the maximum value of the mass-to-size ratio in the scalar-tensor theories. Hereafter, we refer to $(g_{\mu\nu}, \phi)$ and $(g_{*\mu\nu}, \varphi)$, respectively, as the physical frame and the Einstein frame.

3.1 A modified Buchdahl inequality in scalar-tensor theories

In the Einstein frame, a line element of the static and spherically symmetric space-time is written as [10]

$$ds_*^2 = -f_*(r)dt^2 + h_*(r)dr^2 + r^2d\Omega^2. \quad (3.1)$$

The stress-energy tensor for the perfect fluid in the Einstein frame is given by

$$T_*^{\mu\nu} = (\rho_* + p_*)u_*^\mu u_*^\nu + p_*g_*^{\mu\nu}, \quad u_{*\alpha} = -\sqrt{f_*(r)}(dt)_\alpha, \quad (3.2a)$$

where u_*^α is the four velocity of the matter. The stress-energy tensor for the perfect fluid in the physical frame is given by

$$T^{\mu\nu} = (\rho + p)u^\mu u^\nu + pg^{\mu\nu}, \quad u_\alpha = -A\sqrt{f_*(r)}(dt)_\alpha, \quad (3.2b)$$

where u^α is the four velocity of the matter. Fluid variables in the physical and Einstein frames are related according to

$$u^\alpha = u_*^\alpha A^{-1}(\varphi), \quad (3.3)$$

$$\rho = \rho_* A^{-4}(\varphi), \quad (3.4)$$

$$p = p_* A^{-4}(\varphi). \quad (3.5)$$

Now the field equations (2.8) and (2.9) are reduced to the following equations:

$$(r(1 - h_*^{-1}))' = 8\pi G_* \rho_* r^2 + \frac{r^2}{h_*} \varphi'^2, \quad (3.6)$$

$$-r^{-2} h_* (1 - h_*^{-1}) + r^{-1} f_*^{-1} f_*' = 8\pi G_* p_* h_* + \varphi'^2, \quad (3.7)$$

$$\left(\frac{f_*'}{2f_*}\right)' + \left(\frac{f_*'}{2f_*}\right)^2 + \frac{1}{r} \frac{f_*'}{2f_*} - \frac{h_*'}{2h_*} \frac{f_*'}{2f_*} - \frac{1}{r} \frac{h_*'}{2h_*} = 8\pi G_* p_* h_* - \varphi'^2, \quad (3.8)$$

$$r^{-2} (f_* h_*)^{-\frac{1}{2}} \left(\left(\frac{f_*}{h_*}\right)^{\frac{1}{2}} r^2 \varphi' \right)' = 4\pi G_* \alpha(\varphi) (\rho_* - 3p_*), \quad (3.9)$$

where a prime denotes differentiation with respect to r . As is often done in the cases of general relativity, we define a *mass function*, $m_*(r)$, in the Einstein frame as follows:

$$h_*(r) \equiv \left[1 - \frac{2m_*(r)}{r} \right]^{-1}. \quad (3.10)$$

Then (3.6) is rewritten as

$$m_*'(r) = 4\pi G_* \rho_{\text{eff}} r^2, \quad (3.11)$$

where

$$\rho_{\text{eff}} \equiv \rho_* + \frac{\varphi'^2}{8\pi G_* h_*}. \quad (3.12)$$

That is, ρ_{eff} plays the role of an effective density in the Einstein frame.

In order to derive a modified Buchdahl inequality, we assume

$$h_*(r) \geq 0, \quad (3.13)$$

$$f_*(r) \geq 0, \quad (3.14)$$

$$\rho_{\text{eff}}(r) \geq 0, \quad (3.15)$$

$$\rho'_{\text{eff}}(r) \leq 0. \quad (3.16)$$

These assumptions imply the following:

- No black hole exists in the Einstein frame.
- The effective density, ρ_{eff} , is a positive and monotonously decreasing function of the radius.

Moreover, we assume that an interior solution of the above field equations smoothly matches the corresponding exterior one. Note that these assumptions are concerned with the unphysical variables and that their validity should be examined. This will be done later.

Using the assumption (3.16), it is easy to verify the following inequality:

$$\left(\frac{m_*}{r^3}\right)' \leq 0. \quad (3.17)$$

Moreover, with (3.7), (3.8) and (3.11), we obtain

$$-\left(\frac{(\sqrt{f_*})'}{r\sqrt{h_*}}\right)' = \sqrt{f_*h_*} \left(-\left(\frac{m_*}{r^3}\right)' + 2\frac{\varphi'^2}{rh_*}\right) \geq 0. \quad (3.18)$$

Accordingly, we have

$$\frac{(\sqrt{f_*(r_1)})'}{r_1\sqrt{h_*(r_1)}} \geq \frac{(\sqrt{f_*(r_2)})'}{r_2\sqrt{h_*(r_2)}}, \quad r_1 \leq r_2. \quad (3.19)$$

Now let the inequality (3.19) be reformulated in terms of variables of the exterior solution. The exterior solution, whose derivation is given in Appendix B, is

$$ds_*^2 = -e^{\gamma(x)} dt^2 + e^{-\gamma(x)} d\chi^2 + e^{\lambda(x)-\gamma(x)} d\Omega^2, \quad (3.20)$$

where

$$e^{\lambda(x)} = \chi^2 - a\chi, \quad (3.21)$$

$$e^{\gamma(x)} = \left(1 - \frac{a}{\chi}\right)^{\frac{b}{a}}, \quad (3.22)$$

$$\varphi(\chi) = \varphi_0 + \frac{c}{a} \ln \left(1 - \frac{a}{\chi}\right). \quad (3.23)$$

Here a , b , c and φ_0 are constants of integration, and φ_0 is the asymptotic value of φ at infinity. Moreover, the constants, a , b and c , must satisfy the following relation (Appendix B):

$$a^2 - b^2 = 4c^2. \quad (3.24)$$

One may expect that $\chi = a$ is an event horizon. However, this is not the case in generic scalar-tensor theories, where the null surface, $\chi = a$, is a curvature singularity in the Einstein

frame. The singular nature of the unphysical space-time at $\chi = a$ can also be seen when transformation to the Schwarzschild coordinate is made. The Schwarzschild coordinate, r , and the Just coordinate, χ , are related by the following relation:

$$r = \chi \left(1 - \frac{a}{\chi}\right)^{\frac{a-b}{2a}}. \quad (3.25)$$

One finds that, when $a \neq b$, $\chi = a$ in the Just coordinate corresponds to $r = 0$ in the Schwarzschild coordinate.

By matching the interior solution to the exterior solution, we obtain the following relations:

$$r_s = \chi_s \left(1 - \frac{a}{\chi_s}\right)^{\frac{a-b}{2a}}, \quad (3.26)$$

$$f_*(r_s) = \left(1 - \frac{a}{\chi_s}\right)^{\frac{b}{a}}, \quad (3.27)$$

$$h_*(r_s) = \left(1 - \frac{a}{\chi_s}\right) \left(1 - \frac{a+b}{2\chi_s}\right)^{-2}, \quad (3.28)$$

where the subscript, s , refers to χ evaluated at the surface, $r = r_s$. Note that

$$\chi_s > a \geq b. \quad (3.29)$$

Since $h_*(r)^{-1} = 1 - 2m_*(r)/r$, (3.28) becomes

$$2m_*(r_s) = \left(b - \frac{(a+b)^2}{4\chi_s}\right) \left(1 - \frac{a}{\chi_s}\right)^{-\frac{(a+b)}{2a}}. \quad (3.30)$$

Accordingly, by virtue of the positivity of $m_*(r)$, we obtain the additional inequality

$$b - \frac{(a+b)^2}{4\chi_s} > 0. \quad (3.31)$$

With (3.19) and (3.25) ~ (3.28), we obtain the following relation for $r \leq r_s$:

$$\frac{(\sqrt{f_*})'}{r\sqrt{h_*}} \geq \frac{(\sqrt{f_*(r_s)})'}{r_s\sqrt{h_*(r_s)}} = \frac{b}{2r_s^3}. \quad (3.32)$$

Integrating (3.32) from the center, $r = 0$, to the surface, $r = r_s$, we obtain

$$\begin{aligned} 0 &\leq \sqrt{f_*(0)} \\ &\leq \sqrt{f_*(r_s)} - \frac{b}{2r_s^3} \int_0^{r_s} r \sqrt{h_*(r)} dr \\ &\leq \sqrt{f_*(r_s)} - \frac{b}{2r_s^3} \int_0^{r_s} r \left(1 - \frac{2m_*(r_s)}{r_s^3} r^2\right)^{-\frac{1}{2}} dr \\ &= \left(1 - \frac{a}{\chi_s}\right)^{\frac{b}{2a}} + \frac{b}{4m_*(r_s)} \left(\sqrt{1 - \frac{2m_*(r_s)}{r_s}} - 1\right), \end{aligned} \quad (3.33)$$

where the inequality (3.17) has been used.

The inequalities obtained to this point can be simplified in terms of new parameters defined by

$$a_s \equiv \frac{a}{\chi_s}, \quad b_s \equiv \frac{b}{\chi_s}, \quad c_s \equiv \frac{c}{\chi_s}. \quad (3.34)$$

Substituting (3.30) into (3.33), we obtain the following inequality:

$$\begin{aligned} 0 &\leq \sqrt{f_*(0)} \\ &\leq \frac{1}{2}(1-a_s)^{\frac{b_s}{2a_s}} \left(b_s - \frac{(a_s+b_s)^2}{4} \right)^{-1} \times \\ &\quad \times \left[2b_s - \frac{(a_s+b_s)^2}{2} - b_s \sqrt{1-a_s} \left(1 - \sqrt{1 - \frac{4b_s - (a_s+b_s)^2}{4(1-a_s)}} \right) \right]. \end{aligned} \quad (3.35)$$

The above inequality can be further simplified, and we finally obtain a modified Buchdahl inequality in the scalar-tensor theories as

$$F(a_s, b_s) \equiv 3b_s - \frac{1}{2}(a_s + b_s)(a_s + 2b_s) - b_s \sqrt{1-a_s} \geq 0, \quad (3.36)$$

supplemented with (3.29) and (3.31).

The modified Buchdahl inequality can be solved to yield

$$\left. \begin{aligned} b_s \leq a_s \leq 2\sqrt{b_s} - b_s &\quad \text{for } 0 \leq b_s \leq 4(3-2\sqrt{2}), \\ b_s \leq a_s \leq 2\sqrt{2b_s} - 2b_s &\quad \text{for } 4(3-2\sqrt{2}) \leq b_s \leq \frac{8}{9}, \\ \text{Forbidden} &\quad \text{for } b_s > \frac{8}{9}. \end{aligned} \right\} \quad (3.37)$$

Fig. 1 displays the allowed region, D , of (a_s, b_s) .

In addition, we can obtain, with (3.24), the following upper limit on $|c_s|$:

$$|c_s| \leq \frac{2\sqrt{3}}{9}. \quad (3.38)$$

The inequality (3.37) is significant. The third inequality of (3.37) gives us a necessary condition for a spherical star to exist and is reduced to Buchdahl's theorem in general relativity when $c = 0$, i.e., $a = b$, and, accordingly, $\chi = r$. In this case, we have ($R = r_s$)

$$c_s = 0 \iff a_s = b_s = \frac{2M}{R} \leq \frac{8}{9}, \quad (3.39)$$

where M is the ADM mass defined at spatial infinity, and R is related to the surface area, S , as $S = 4\pi R^2$.

The new and important inequality (3.38) is characteristic of the scalar-tensor theories and does not have a general relativistic counterpart. It has been found the appearance of non-perturbative behavior of the scalar field in the previous numerical studies [6],[7]. Our result implies that, even in a strong gravitational field, the characteristic amplitude of the scalar field, $|c_s|$, is bounded.

It is important to note that we have not used any assumption regarding the coupling function, $A(\varphi)$, in deriving the inequalities. In particular, the inequalities (3.37) and (3.38) give theory-independent constraints on the parameters, b_s and c_s .

3.2 The mass-to-size ratio

Now we reformulate the inequalities derived in the previous section, which are in terms of variables in the Einstein frame, in order to obtain the mass-to-size ratio in the physical frame. To do this, the coupling function, $A(\varphi)$, should be specified. In this paper, we assume as an example of this coupling function the simple form

$$A(\varphi) = e^{\frac{1}{2}\beta\varphi^2}, \quad (3.40)$$

where β is a constant[6],[7]. Then the coupling strength, $\alpha(\varphi)$, becomes

$$\alpha(\varphi) = \beta\varphi. \quad (3.41)$$

A natural definition of the radius of a spherical star is obtained by using its (physical) surface area as follows. In the physical frame, the surface area, S , is given by

$$\begin{aligned} S &= 4\pi A^2(\varphi_s) e^{\lambda(\chi_s) - \gamma(\chi_s)} \\ &= 4\pi \chi_s^2 (1 - a_s)^{1 - \frac{b_s}{a_s}} \exp \left[\beta \left(\frac{c_s}{a_s} \ln(1 - a_s) \right)^2 \right], \end{aligned} \quad (3.42)$$

where we take the asymptotic value of the scalar field as $\varphi_0 = 0$, and, accordingly, we have $A(\varphi_0) = 1$ and $\alpha(\varphi_0) = 0$. This surface area defines the physical radius, R , of the star in a similar manner as in general relativity:

$$R \equiv \sqrt{\frac{S}{4\pi}}. \quad (3.43)$$

When $\varphi_0 = 0$, the effective gravitational constant, G , defined in Appendix A, is equal to G_* . If $\varphi_0 \neq 0$, contributions of the scalar field appear in the above expression of R in terms of $c\beta\varphi_0$.

The definition of the mass in the Brans-Dicke theory is found in Ref.[12], and the mass in the scalar-tensor theories is defined in the same manner. In defining the mass, the metric should be expressed in the isotropic coordinate, \bar{r} , which is related to χ as

$$\chi = \bar{r} \left(1 + \frac{a}{4\bar{r}} \right)^2. \quad (3.44)$$

In our model, the exterior solution is then rewritten in terms of \bar{r} as

$$\begin{aligned} ds^2 &= A^2(\varphi) \left[- \left(\frac{1 - \frac{a}{4\bar{r}}}{1 + \frac{a}{4\bar{r}}} \right)^{\frac{2b}{a}} dt^2 + \left(1 + \frac{a}{4\bar{r}} \right)^{\frac{2(a+b)}{a}} \left(1 - \frac{a}{4\bar{r}} \right)^{\frac{2(a-b)}{a}} (d\bar{r}^2 + \bar{r}^2 d\Omega^2) \right] \\ G_*\phi &= A^{-2}(\varphi) = \exp \left[- \frac{4\beta c^2}{a^2} \left(\ln \frac{1 - \frac{a}{4\bar{r}}}{1 + \frac{a}{4\bar{r}}} \right)^2 \right]. \end{aligned} \quad (3.45)$$

By introducing the asymptotic Cartesian coordinates such that $\bar{r} = \sqrt{(x^1)^2 + (x^2)^2 + (x^3)^2}$, the asymptotic form of the solution is easily found to be

$$\begin{aligned} G_*\phi &\sim 1 + \frac{0}{\bar{r}} \equiv 1 + \frac{2M_S}{\bar{r}}, & g_{00} &\sim -1 + \frac{b}{\bar{r}} \equiv -1 + \frac{2(M_T + M_S)}{\bar{r}}, \\ g_{ij} &\sim \left(1 + \frac{b}{\bar{r}} \right) \delta_{ij} \equiv \left(1 + \frac{2(M_T - M_S)}{\bar{r}} \right) \delta_{ij}, \end{aligned} \quad (3.46)$$

where the quantities, M_S and M_T , are called, respectively, the scalar mass and the tensor mass. At Newtonian order, their sum, $M \equiv M_T + M_S$, plays the role of the mass and is called the active gravitational mass. In our model, $M_S = 0$, and, accordingly, $M_T = M = b/2$. Hereafter, we call M the mass for simplicity.

Now we are ready to calculate the mass-to-size ratio in the scalar-tensor theory as a function of a_s , b_s , χ_s and a specific parameter of our model, β . We obtain

$$H(a_s, b_s; \beta) \equiv \frac{b}{R} = b_s(1 - a_s)^{\frac{b_s - a_s}{2a_s}} \exp \left[-\frac{1}{2}\beta \left(\frac{c_s}{a_s} \ln(1 - a_s) \right)^2 \right]. \quad (3.47)$$

In Fig.2, in the allowed region of (a_s, b_s) , we display lines on which $H(a_s, b_s; \beta)$ is equal to $8/9$ for various values of β . For a fixed value of β , the region above the line corresponds to the case that the mass-to-size ratio, $2M/R$, exceeds Buchdahl's limit, $8/9$. Moreover, in some cases, it may be greater than unity. We refer to this case as the *black hole limit*. The maximum values of $H(a_s, b_s; \beta)$ for various values of β are shown in Fig.3. Indeed, the maximum mass-to-size ratio can sometimes become larger than the black hole limit. However, the physical exterior solution generically does not have an event horizon in scalar-tensor theories, in contrast to general relativity, and, therefore, the condition, $2M/R > 1$, does not imply the existence of a black hole.

Now suppose that a space rocket approaches a star for which $2M/R > 1$ and goes into its *Schwarzschild radius* defined by $2M$. A spaceman in the rocket would be resigned to his fate to die, but we know that he still has a chance to return alive from a *false black hole*.

4 Numerical results

Equations (3.6) ~ (3.9) are numerically solved to obtain an interior solution. This solution is then matched to the exterior one, and numerical values of the parameters a_s , b_s and c_s are calculated. Some details of the numerical methods are summarized in Appendix C. Since we take $\varphi_0 = 0$, G_* is equal to G (Appendix A). Hereafter, we use units in which $G_* = G = 1$.

As for the matter, we assume the following polytropic equation of state [13]:

$$\rho = m_b n + \frac{K n_0 m_b}{\Gamma - 1} \left(\frac{n}{n_0} \right)^\Gamma, \quad (4.1)$$

$$p = K m_b n_0 \left(\frac{n}{n_0} \right)^\Gamma, \quad (4.2)$$

$$m_b = 1.66 \times 10^{-24} \text{ g}, \quad (4.3)$$

$$n_0 = 0.1 \text{ fm}^{-3}. \quad (4.4)$$

We take the parameters values, $\Gamma = 2.34$ and $K = 0.0195$ [6], which fit a realistic equation of state of high density nuclear matter, and probably also that of a neutron star quite well. Our numerical solutions are therefore parametrized by β and $n_c \equiv n(0)$. It has been shown numerically that significant effects of φ appear when $\beta \leq -4.35$ [6],[7], and we are mostly interested in cases of negative values of β . In cases of positive values of β , we cannot numerically find any significantly different behavior of the solutions compared with those in general relativity, and any further discussion in these cases is no longer done.

First, we examine whether our assumption, $\rho'_{\text{eff}} \leq 0$, is satisfied. In Fig.4, we give an example of numerical behavior of the effective density for $\beta = -5$ and $n_c/n_0 = 10$. Including

this case, we find that the assumption, $\rho'_{\text{eff}}(r) \leq 0$, is mostly satisfied, as summarized in the 3rd column of Table 1. Differentiating (3.12), we obtain

$$\rho'_{\text{eff}} = A^4(\varphi)\rho' + 4A^4(\varphi)\alpha(\varphi)\varphi'\rho + \left(\frac{\varphi'^2}{8\pi G_* h_*}\right)'. \quad (4.5)$$

In Fig.5, we show the 1st, 2nd and 3rd terms in (4.5) with the same parameters as Fig.4. The first term is indeed dominant and always negative. In Fig.6, we compare the corresponding physical quantities, $\rho(r)$ and $\phi(r)$, and the unphysical scalar field, $\varphi(r)$. It is found that the *local gravitational constant*, $G(\phi) \equiv 1/\phi$, increases as ρ decreases toward the surface. However, this behavior is strongly dependent on the coupling function, and the sign of β is crucial in the present case.

Next, we examine an extreme example in which the assumption, $\rho'_{\text{eff}} \leq 0$, is violated. Fig.7 shows the effective density, ρ_{eff} , for $\beta = -30$ and $n_c/n_0 = 10$. It is seen that ρ_{eff} remains constant in the central part and then increases between the two rectangles in Fig.7. In Fig.8, we show the three terms in (4.5) and find that the positive second term becomes partially dominant. Again, this behavior is strongly dependent on the coupling function. In the present case, we have $\alpha(\varphi) = \beta\varphi$, where $\beta < 0$. Therefore, when $\varphi' < 0$ and $|\beta|$ is large, such that the second term in (4.5) is dominant, ρ'_{eff} becomes positive, and the assumption is violated. In Fig.9, we compare $\rho(r)$, $\phi(r)$ and $\varphi(r)$. It is found that, despite small values of φ , ϕ can be large due to a large value of $|\beta|$. However, it should be noted that this assumption is concerned with the unphysical quantity, ρ_{eff} , and that its violation does not necessarily mean that this extreme case is unreal. In Fig.10, we show the energy density, $\rho(r)$, and the pressure, $p(r)$, in the physical frame in the extreme case: $\beta = -30$, $n_c/n_0 = 10$. The behavior of these quantities seems ordinary, that is, they are monotonously decreasing functions of r . Accordingly, one may think that this can be a physically acceptable equilibrium solution despite the violation of the assumption, $\rho'_{\text{eff}} \leq 0$. However, we are forbidden to take β smaller than -5 because of experimental constraints (Appendix A, [7],[14]).

For each value of β , the mass-to-size ratio, $2M/R = H(a_s, b_s; \beta)$, can be numerically calculated as a function of n_c . By changing n_c , we search for a maximum value of $H(a_s, b_s; \beta)$ for each β . In the 5th column of Table1, we summarize our results for the maximum mass-to-size ratio, where the parameters are chosen such that the assumption, $\rho'_{\text{eff}} \leq 0$, is satisfied. For $\beta < -12.07$, we find numerically that the assumption is always violated. The first interesting example is found in the case, $\beta = -12.07$, in which the maximal mass-to-size ratio is obtained as $H_{\text{MAX}} = 1.018$ when $n_c/n_0 = 11.2$. This is a case in which H_{MAX} exceeds the black hole limit, $H = 1$. Another interesting example is found in the case, $\beta = -11$, in which $H_{\text{MAX}} = 0.919$ when $n_c/n_0 = 11.3$. This is a case in which H_{MAX} exceeds Buchdahl's limit, $H = 8/9 \approx 0.889$. These examples have academic importance in the sense that our analytic results in the previous section are partially realized also in the numerical solutions.

To this point, the stability of our numerical solutions has not been taken into account. We have found that $\rho - 3p$ may be a good estimator of the stability, as described below. The baryonic mass of a star is defined as [6]

$$\bar{m} = m_b \int_0^{r_s} 4\pi n A^3(\varphi) r^2 \left(1 - \frac{2m_*}{r}\right)^{-\frac{1}{2}} dr. \quad (4.6)$$

We have numerically examined how \bar{m} depends on n_c and find a significant correlation between the signature of $d\bar{m}/dn_c$ and that of $\rho - 3p$. That is, the cases, $\rho - 3p < 0$ and $\rho - 3p > 0$, approximately correspond to the cases, $d\bar{m}/dn_c < 0$ and $d\bar{m}/dn_c > 0$, respectively. Accordingly, we shall interpret the signature of $\rho - 3p$ as a measure of the onset of the instability in

our numerical calculations. When we impose the condition, $\rho - 3p \geq 0$, we cannot numerically find cases in which H_{MAX} exceeds Buchdahl's limit, as is seen in the 4th and 5th columns in Table 1. Note that the condition, $\beta < -5$, also excludes all the interesting cases in which H_{MAX} exceeds Buchdahl's limit.

Let us find a critical value, $\beta_c < 0$, of β , such that, for $\beta < \beta_c$, nonlinear behavior of the scalar field begins to appear. We numerically calculated a_s , b_s and c_s as functions of n_c for $\beta = -4, -5$ and -6 under the conditions, $\rho'_{\text{eff}} \leq 0$ and $\rho - 3p \geq 0$. We show (a_s, b_s) and c_s in Fig.11 and Fig.12, respectively. For $\beta \geq -4$, almost no deviation from general relativity appears. In the cases that $\beta = -5$ and -6 , these parameters show deviations from general relativity in which $a_s = b_s$ and $c_s = 0$. Our results are consistent with the previous works [6],[7], in which β_c is found to be -4.35 . Note that, even when $\beta < \beta_c$, our inequality, $|c_s| \leq 2\sqrt{3}/9$, is surely satisfied. This reconfirms our assertion that the nonlinear effects are always bounded in this sense.

Now we shall briefly compare our numerical results with those in previous works [6],[7]. The maximum baryonic mass of a star is defined as the peak of the $\bar{m}-n_c$ relation. We numerically found that the maximum baryonic mass increases from the general relativistic value, $2.23M_\odot$, to $2.38M_\odot$ and $2.96M_\odot$ for $\beta = -5$ and -6 , respectively. The corresponding radius defined by (3.43) also increases from the general relativistic value, 11.0 km, to 12.0 km and 12.9 km for $\beta = -5$ and -6 , respectively. In Ref.[6], a fractional binding energy, $f_{\text{BE}} \equiv 2\bar{m}/b - 1$, is used as a measure of the scalar field contribution to the mass. We numerically found that the maximum value of f_{BE} increases from the general relativistic value, $f_{\text{BE}} = 0.14$, to $f_{\text{BE}} = 0.16$ and 0.22 for $\beta = -5$ and -6 , respectively. Though a slightly different asymptotic value of φ_0 has been adopted in Ref.[6], these results are consistent with the previous results.

The mass-size relation of neutron stars has been thoroughly studied in general relativity by solving the Oppenheimer-Volkoff equation, and it has been found numerically that, as the equation of state becomes softer, the mass-to-size ratio becomes larger when its mass is fixed[13]. In Fig.13, we compare, under the condition, $\rho - 3p \geq 0$, the relations between the mass-to-size ratio and the mass in general relativity and in scalar-tensor theories. It is seen in Fig.13 that the deviation from general relativity due to the scalar field begins appearing for $M > 1.2M_\odot$. When $M < 1.7M_\odot$ ($M > 1.7M_\odot$), our numerical solutions in the scalar-tensor theory correspond to the solutions in general relativity with the softer (stiffer) equation of state. The mass of PSR1913+16 has been evaluated as $1.4M_\odot$ [13], and, if the adopted equation of state is adequate, the scalar field contribution to the mass-to-size ratio is negligibly small when $\beta > -5$. Further discussion on the equation of state is left as a future work.

Finally, we shall derive a redshift formula in the scalar-tensor theories. A null vector, k^μ , tangent to the radial null geodesic, and a four-velocity, U^μ , of a static observer are, respectively, given by

$$k^\mu = A^{-2}(e^{-\gamma}, 1, 0, 0), \quad U^\mu = (A^{-1}e^{-\gamma/2}, 0, 0, 0), \quad U^\mu U_\mu = -1. \quad (4.7)$$

The frequency, ω , of a light ray is given by

$$\omega = -g_{\mu\nu}k^\mu U^\nu = A^{-1}e^{-\gamma/2}. \quad (4.8)$$

The redshift, z , is then obtained as

$$1 + z = \frac{\omega_{\text{source}}}{\omega_{\text{observer}}} = A^{-1}e^{-\gamma/2} \Big|_{\text{source}}, \quad (4.9)$$

where the observer is assumed to be at the spatial infinity, $a/\chi \rightarrow 0$. By using (3.22),(3.23)

and (3.40), we obtain the redshift formula in the present specific scalar-tensor theory as

$$1 + z = (1 - a_s)^{-\frac{b_s}{2a_s}} \exp \left\{ -\frac{1}{2}\beta \left[\frac{c_s}{a_s} \ln(1 - a_s) \right]^2 \right\} = \frac{1}{b_s} (1 - a_s)^{\frac{a_s - 2b_s}{2a_s}} \left(\frac{2M}{R} \right). \quad (4.10)$$

The maximum value of z depends on β and the parameters, a_s and b_s , in the allowed region, D , in Fig.1. Theoretically, the possible maximum value of z , z_{\max} , is obtained as $z_{\max} = 2$ in general relativity and $z_{\max} = 164$ and 356 for $\beta = -5$ and $\beta = -6$, respectively. We compare these values with those obtained in the numerical calculations under the condition, $\rho - 3p \geq 0$. We numerically find that $z_{\max} = 0.43$ in general relativity, and that $z_{\max} = 0.44$ and 0.55 for $\beta = -5$ and -6 , respectively. In our numerical solutions with the presently adopted model parameters, the deviation of the redshift formula from that in general relativity remains small compared with the theoretically possible deviation. However, the redshift difference, 0.01 , numerically found for $\beta = -5$ may be detectable. Therefore the redshift measurement of neutron stars will provide us with a possible tool for the experimental test of general relativity.

5 Summary

We have derived a modified Buchdahl inequality in scalar-tensor theories of gravity. As a result, we have obtained two theory-independent inequalities, $b_s \leq 8/9$ and $|c_s| \leq 2\sqrt{3}/9$. The first inequality corresponds to the Buchdahl inequality in general relativity. The second inequality is characteristic of scalar-tensor theories. Consequently, even if the scalar field is locally amplified due to non-perturbative effects in a strong gravitational field, the characteristic amplitude of the scalar field, $|c_s|$, is bounded in this sense.

The modified Buchdahl inequality is then reformulated to obtain a theory-dependent mass-to-size ratio, $2M/R$, with an example of the coupling function, $A(\varphi)$, in a simple form. If we take $\varphi_0 = 0$, the mass in the physical frame is the same as that in general relativity, $M = b/2$. However, the physical radius, R , of the star can be smaller than the general relativistic one. As a result, the mass-to-size ratio can exceed not only Buchdahl's limit but also the black hole limit in contrast to general relativity.

Our analytic results have been numerically confirmed when we assume a polytropic equation of state for the matter. In particular, we have found numerical solutions in which the mass-to-size ratio exceeds both Buchdahl's limit and the black hole limit. However, these theoretically interesting stars could not be found numerically under the condition, $\rho - 3p \geq 0$, which is interpreted as a numerical measure of the onset of the instability of a star. Moreover, under this condition, we find numerically that any quantitative deviation from general relativity due to the scalar field remains comparatively small in contrast to our analytic results, where possible significant effects of the scalar field are expected. However, as discussed briefly, some measurable effects in astronomical observations may exist.

Now suppose that a space rocket approaches a massive star for which $2M/R \gg 1$. If the rocket accidentally goes into a *Schwarzschild radius* of the star defined by $2M$, a spaceman in the rocket would be resigned to his fate to die. Now we know that, unfortunately for him, even if scalar-tensor theories describe classical gravity, he would hardly have a chance to return alive, because he could hardly meet a real *false black hole*. He has two possible futures, and they are equally tragic:

- If it is a black hole in terms of general relativity, he can never escape.

- If it is a naked singularity in terms of scalar-tensor theories, nobody knows what will happen when he touches it.

Acknowledgements

The authors would like to thank Dr. K. Oohara for useful discussions regarding numerical calculations. They also thank the referee for his careful reading of the manuscript and valuable comments.

A Observational constraints

In general, the coupling strength, $\alpha(\varphi)$, can be an arbitrary function of φ , and in the limit, $\alpha(\varphi) \rightarrow 0$, scalar-tensor theories approach general relativity. One defines

$$\alpha_0 \equiv \alpha(\varphi_0), \quad (\text{A.1})$$

$$\beta_0 \equiv \left. \frac{d\alpha(\varphi)}{d\varphi} \right|_{\varphi=\varphi_0}, \quad (\text{A.2})$$

where φ_0 is the asymptotic value of φ at spatial infinity. In the post-Newtonian approximation, the PPN parameters and the effective gravitational constant are expressed as follows [11]:

$$1 - \gamma_E = \frac{2\alpha_0^2}{1 + \alpha_0^2}, \quad (\text{A.3})$$

$$\beta_E - 1 = \frac{\beta_0 \alpha_0^2}{2(1 + \alpha_0^2)^2}, \quad (\text{A.4})$$

$$G = G_* A^2(\varphi_0) (1 + \alpha^2(\varphi_0)). \quad (\text{A.5})$$

General relativity corresponds to the case that $\beta_E = \gamma_E = 1$ [4],[15]. Experiments on the time delay and deflection of light in the solar system constrain $|1 - \gamma_E|$ as [14]

$$|1 - \gamma_E| < 2 \times 10^{-3}, \quad (\text{A.6})$$

which constrains $\omega(\phi)$ and α_0 as

$$\omega > 500, \quad \alpha_0^2 < 10^{-3}. \quad (\text{A.7})$$

The lunar-laser-ranging experiments constrain $|\beta_E - 1|$ as [14]

$$|\beta_E - 1| \lesssim 6 \times 10^{-4}, \quad (\text{A.8})$$

which only constrains some combination of α_0 and β_0 . Consequently, if α_0 tends to zero, the constraint on β_0 is effectively lost. However, by adopting a specific coupling function, $A = \exp(\frac{1}{2}\beta\varphi^2)$, another constraint on β_0 is obtained from observations of the binary-pulsars, PSR1913+16, as [7],[14]

$$\beta_0 > -5. \quad (\text{A.9})$$

When we take (3.40) as a coupling function, the coupling strength is $\alpha(\varphi) = \beta\varphi$. Accordingly, $\alpha_0 = \beta\varphi_0$, and we obtain the constraint on φ_0 . In this paper we take $\varphi_0 = 0$ for simplicity.

B An exterior solution

A line element of the Einstein frame in the Just coordinate is [16]

$$ds_* = -e^{\gamma(\chi)} dt^2 + e^{-\gamma(\chi)} d\chi^2 + e^{\lambda(\chi)-\gamma(\chi)} d\Omega^2. \quad (\text{B.1})$$

The field equations in the exterior space-time are

$$\gamma'' + \gamma'\lambda' = 0, \quad (\text{B.2})$$

$$-\gamma'^2 + \gamma'\lambda' - \lambda'^2 + \gamma'' - 2\lambda'' = 4\varphi'^2, \quad (\text{B.3})$$

$$2 + e^\lambda(\gamma'\lambda' - \lambda'^2 + \gamma'' - \lambda'') = 0, \quad (\text{B.4})$$

$$\varphi'' + \lambda'\varphi' = 0, \quad (\text{B.5})$$

where a prime denotes differentiation with respect to χ . With (B.2),(B.4) and (B.5), the exterior solution can be obtained as

$$e^{\lambda(\chi)} = \chi^2 - a\chi, \quad (\text{B.6})$$

$$e^{\gamma(\chi)} = \left(1 - \frac{a}{\chi}\right)^{\frac{b}{a}}, \quad (\text{B.7})$$

$$\varphi(\chi) = \varphi_0 + \frac{c}{a} \ln\left(1 - \frac{a}{\chi}\right), \quad (\text{B.8})$$

where a, b and c are constants of integration, and φ_0 denotes the asymptotic value of φ at infinity. With (B.3), one finds

$$a^2 - b^2 = 4c^2. \quad (\text{B.9})$$

The coordinate transformation between the Schwarzschild coordinate, r , and the Just coordinate, χ , is given by

$$r^2 = \chi^2 \left(1 - \frac{a}{\chi}\right)^{\frac{a-b}{a}}. \quad (\text{B.10})$$

Note that $r \rightarrow \chi$ at spatial infinity. In the Schwarzschild coordinate, a line element becomes

$$ds_*^2 = -e^{2\nu(r)} dt^2 + e^{2\mu(r)} dr^2 + r^2 d\Omega^2. \quad (\text{B.11})$$

The exterior solution in the Schwarzschild coordinate is given by

$$e^{2\nu(r)} = \left(1 - \frac{a}{\chi(r)}\right)^{\frac{b}{a}}, \quad (\text{B.12})$$

$$e^{2\mu(r)} = \left(1 - \frac{a}{\chi(r)}\right) \left(1 - \frac{a+b}{2\chi(r)}\right)^{-2}. \quad (\text{B.13})$$

Asymptotic behavior of the exterior solution at spatial infinity are as follows:

$$e^{2\nu(r)} \longrightarrow 1 - \frac{b}{r}, \quad (\text{B.14})$$

$$e^{2\mu(r)} \longrightarrow 1 + \frac{b}{r}, \quad (\text{B.15})$$

$$\varphi(r) \longrightarrow \varphi_0 - \frac{c}{r}. \quad (\text{B.16})$$

C An interior solution: Numerical methods

Using the variables, $m_*(r)$ and $\nu(r)$, defined by

$$f_*(r) \equiv e^{2\nu(r)}, \quad h_*(r) \equiv \left[1 - \frac{2m_*(r)}{r}\right]^{-1}, \quad (\text{C.1})$$

the field equations (3.6) \sim (3.9) become

$$\frac{dm_*}{dr} = 4\pi G_* A^4(\varphi) r^2 \rho + \frac{1}{2} r (r - 2m_*) \psi^2, \quad (\text{C.2})$$

$$\frac{d\nu}{dr} = \frac{m_* + 4\pi G_* A^4(\varphi) r^3 p}{r(r - 2m_*)} + \frac{1}{2} r \psi^2 \equiv \Phi(r), \quad (\text{C.3})$$

$$\frac{d\varphi}{dr} = \psi, \quad (\text{C.4})$$

$$\frac{d\psi}{dr} = \frac{4\pi G_* A^4(\varphi) r}{r - 2m_*} [\alpha(\varphi)(\rho - 3p) + (\rho - p)r\psi] - \frac{2(r - m_*)}{r(r - 2m_*)} \psi, \quad (\text{C.5})$$

$$\frac{dp}{dr} = -(\rho + p)(\Phi + \alpha(\varphi)\psi). \quad (\text{C.6})$$

The total baryon mass measured in the physical frame is

$$\bar{m} = m_b \int n \sqrt{-g} u^0 d^3x = m_b \int_0^{r_s} 4\pi n A^3(\varphi) r^2 \left(1 - \frac{2m_*}{r}\right)^{-\frac{1}{2}} dr. \quad (\text{C.7})$$

Given the equation of state, we can numerically integrate the above field equations outward from the center, $r = 0$, with the boundary conditions as follows:

$$\left. \begin{aligned} m_*(0) &= 0, \\ \varphi(0) &= \varphi_c, \\ \psi(0) &= 0, \\ p(0) &= p_c, \\ \rho(0) &= \rho_c, \end{aligned} \right\} \quad (\text{C.8})$$

where ρ_c and p_c are given by replacing n in (4.1) and (4.2) with $n_c \equiv n(0)$. The surface of a star, $r = r_s$, is determined by the condition, $p(r_s) = 0$. A numerically obtained interior solution is to be matched to the exterior one by the conditions [6],[7]:

$$\varphi_0 = \varphi_s + \frac{\psi_s}{\sqrt{\nu'_s{}^2 + \psi_s^2}} \tanh^{-1} \left(\frac{\sqrt{\nu'_s{}^2 + \psi_s^2}}{\nu'_s + 1/r_s} \right), \quad (\text{C.9})$$

$$b = 2r_s^2 \nu'_s \sqrt{1 - \frac{2m_{*s}}{r_s}} \exp \left(-\frac{\nu'_s}{\sqrt{\nu'_s{}^2 + \psi_s^2}} \tanh^{-1} \left(\frac{\sqrt{\nu'_s{}^2 + \psi_s^2}}{\nu'_s + 1/r_s} \right) \right), \quad (\text{C.10})$$

$$c = \frac{\psi_s}{2\nu'_s} b, \quad (\text{C.11})$$

$$a = \sqrt{b^2 + 4c^2}, \quad (\text{C.12})$$

where a prime denotes differentiation with respect to r , and the subscript, s , refers to quantities evaluated at the surface, r_s . The central value of φ , φ_c , is chosen such that we have $\varphi_0 = 0$.

References

- [1] C. Brans and R. H. Dicke, *Phys. Rev.* **124**, 925 (1962).
- [2] P. G. Bergmann, *Int. J. Theor. Phys.* **1**, 25 (1968).
- [3] R. V. Wagoner, *Phys. Rev.* **D1**, 3209, (1970).
- [4] C. M. Will, *Theory and Experiment in Gravitational Physics*, (Cambridge University Press, Cambridge, 1993).
- [5] M. B. Green, J. H. Schwartz and E. Witten, *Superstring Theory vols. 1,2*, (Cambridge University Press, Cambridge, 1987).
- [6] T. Damour and G. Esposito-Farèse, *Phys. Rev. Lett.* **70**, 2220 (1993).
- [7] T. Damour and G. Esposito-Farèse, *preprint* gr-qc/9602056.
- [8] H. A. Buchdahl, *Phys. Rev.* **116**, 1027 (1959).
- [9] S. Weinberg, *Gravitation and Cosmology*, (Wiley, New York, 1972).
- [10] R. M. Wald, *General Relativity*, (The University of Chicago Press, Chicago and London, 1984).
- [11] T. Chiba, T. Harada and K. Nakao, *Prog. Theor. Phys. Suppl.* **128**, 335 (1997).
- [12] D. L. Lee, *Phys. Rev.* **D10**, 2374 (1974).
- [13] S. L. Shapiro and S. A. Teukolsky, *Black Holes, White Dwarfs and Neutron Stars*, (Wiley, 1983).
- [14] G. Esposito-Farèse, *preprint* gr-qc/9612039.
- [15] C. W. Misner, K. S. Thorne and J. A. Wheeler, *Gravitation*, (Freeman, San Francisco, 1973).
- [16] T. Damour and G. Esposito-Farèse, *Class. Quant. Grav.* **9**, 2093 (1992).

Figure 1: The allowed region, D , is depicted, where horizontal and vertical axes denote, respectively, b_s and a_s . The characteristic points, $P = (4(3 - 2\sqrt{2}), 4(3\sqrt{2} - 4))$, $Q = (8/9, 8/9)$ and $K = (4/9, 8/9)$, are shown. In general relativity, $a_s = b_s$. Buchdahl's limit is denoted by Q . On K , $|c_s|$ takes the maximum value, $|c_s|_{\text{MAX}} = 2\sqrt{3}/9$.

Figure 2: On each lines, $H(a_s, b_s; \beta) = 8/9$ for various values of β : 0, -3, -5, -10 and -100. Horizontal and vertical axes denote, respectively, b_s and a_s .

Figure 3: The Maximum mass-to-size ratio, H_{MAX} , is shown as a function of β . Horizontal and vertical axes denote, respectively, β , and H_{MAX} . A horizontal line, $H_{\text{MAX}} = 8/9$, denotes Buchdahl's limit in general relativity. When $\beta \lesssim 0.4$, H_{MAX} exceeds Buchdahl's limit. When $\beta \lesssim 0.2$, H_{MAX} exceeds unity, a black hole limit.

Figure 4: The effective density, $\rho_{\text{eff}}(r)$, is shown in the case that $\beta = -5$ and $n_c/n_0 = 10$. Horizontal and vertical axes denote, respectively, the radial coordinate, r , in the unit of 10km, and the effective density, $\rho_{\text{eff}}(r)/(m_b n_0)$. It is seen that the assumption, $\rho'_{\text{eff}}(r) \leq 0$, is satisfied.

Figure 5: Each term of (4.5) in $\rho'_{\text{eff}}(r)$ is shown for $\beta = -5$ and $n_c/n_0 = 10$. Horizontal and vertical axes denote, respectively, the radial coordinate, r , in the unit of 10km, and the 1st, 2nd and 3rd terms in (4.5).

Figure 6: We compare $\phi(r)$, $\rho(r)$ and $\varphi(r)$ in the case that $\beta = -5$ and $n_c/n_0 = 7.9$. Horizontal and vertical axes denote, respectively, the radial coordinate, r , in the unit of 10km, and $\rho(r)/(m_b n_0)$, $\phi(r)$ and $\varphi(r)$. On a thin dotted line, $G \equiv 1/\phi_0 = 1$, i.e., general relativity.

Figure 7: The effective density, $\rho_{\text{eff}}(r)$, is shown in the case that $\beta = -30$ and $n_c/n_0 = 10$. Horizontal and vertical axes denote, respectively, the radial coordinate, r , in the unit of 10km, and the effective density, $\rho_{\text{eff}}(r)/(m_b n_0)$. It is seen that the assumption, $\rho'_{\text{eff}}(r) \leq 0$, is partially violated between two rectangles.

Figure 8: Each term of (4.5) in $\rho'_{\text{eff}}(r)$ is shown for $\beta = -30$ and $n_c/n_0 = 10$. Horizontal and vertical axes denote, respectively, the radial coordinate, r , in the unit of 10km, and the 1st, 2nd and 3rd terms in (4.5).

Figure 9: We compare $\phi(r)$, $\rho(r)$ and $\varphi(r)$ in the case that $\beta = -30$ and $n_c/n_0 = 10$. Horizontal and vertical axes denote, respectively, the radial coordinate, r , in the unit of 10km, and $\rho(r)/(m_b n_0)$, $\phi(r)$ and $\varphi(r)$. On a thin dotted line, $G \equiv 1/\phi_0 = 1$, i.e., general relativity.

Figure 10: We show $\rho(r)$ and $p(r)$ in the physical frame for $\beta = -30$ and $n_c/n_0 = 10$. Horizontal and vertical axes denote, respectively, the radial coordinate, r , in the unit of 10km, and $\rho(r)/(m_b n_0)$ and $p(r)/(m_b n_0)$. Though the assumption, $\rho'_{\text{eff}}(r) \leq 0$, is violated in the Einstein frame, the conditions, $\rho(r) - 3p(r) \geq 0$, $\rho'(r) \leq 0$ and $p'(r) \leq 0$ are all satisfied in the physical frame.

Figure 11: We show the parameters, (a_s, b_s) , in each equilibrium solution for $n_c/n_0 = 2.5 \sim 10.3$. We take $\beta = -4, -5$ and -6 , and impose the conditions, $\rho(r) - 3p(r) \geq 0$ and $\rho'_{\text{eff}}(r) \leq 0$. Horizontal and vertical axes denote, respectively, b_s and a_s .

Figure 12: We show the parameter, c_s , in each equilibrium solution for $n_c/n_0 = 1.0 \sim 10.3$. We take $\beta = -4, -5$ and -6 , and impose the conditions, $\rho(r) - 3p(r) \geq 0$ and $\rho'_{\text{eff}}(r) \leq 0$. Horizontal and vertical axes denote, respectively, n_c/n_0 and c_s . A horizontal thin dotted line denotes the limit on c_s , i.e., $c_s = -2\sqrt{3}/9$.

Figure 13: We show the relation between the mass-to-size ratio and the mass. We take $\beta = -5$ and -6 , and impose the conditions, $\rho(r) - 3p(r) \geq 0$ and $\rho'_{\text{eff}}(r) \leq 0$. Horizontal and vertical axes denote, respectively, M/M_\odot , and $2M/R$. The solid line represents the mass-to-size ratio in general relativity.

β	n_c/n_0	$\rho'_{\text{eff}} \leq 0$	$\rho - 3p \geq 0$	H_{max}
-12.07	0.1 ~ 10.3	○	○	0.679
	10.3 ~ 11.2	○	×	1.018
-11.0	0.1 ~ 10.3	○	○	0.666
	10.3 ~ 11.3	○	×	0.919
-10.0	0.1 ~ 10.3	○	○	0.651
	10.3 ~ 11.4	○	×	0.834
-6.0	0.1 ~ 10.3	○	○	0.556
	10.3 ~ 11.2	○	×	0.569
-5.0	0.1 ~ 10.3	○	○	0.517
	10.3 ~ 15.7	○	×	0.567
-4.0	0.1 ~ 10.3	○	○	0.514
	10.3 ~ 14.9	○	×	0.562
0.0	0.1 ~ 10.3	○	○	0.514
	10.3 ~ 14.9	○	×	0.562

Table 1: We summarize our numerical results. In the 1st column, β is given. In the 2nd column, we give a range of n_c from our numerical studies. In the 3rd and 4th columns, we indicate, respectively, whether the assumption, $\rho'_{\text{eff}} \leq 0$, and the condition, $\rho - 3p \geq 0$, are satisfied. In the 5th column, the maximum mass-to-size ratio is shown for each β .

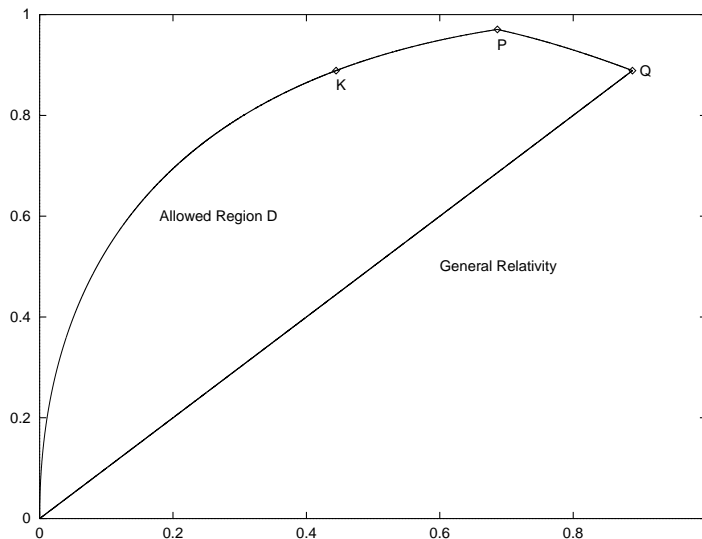


Figure 1: The allowed region, D , is depicted, where horizontal and vertical axes denote, respectively, b_s and a_s . The characteristic points, $P = (4(3 - 2\sqrt{2}), 4(3\sqrt{2} - 4))$, $Q = (8/9, 8/9)$ and $K = (4/9, 8/9)$, are shown. In general relativity, $a_s = b_s$. Buchdahl's limit is denoted by Q . On K , $|c_s|$ takes the maximum value, $|c_s|_{\text{MAX}} = 2\sqrt{3}/9$.

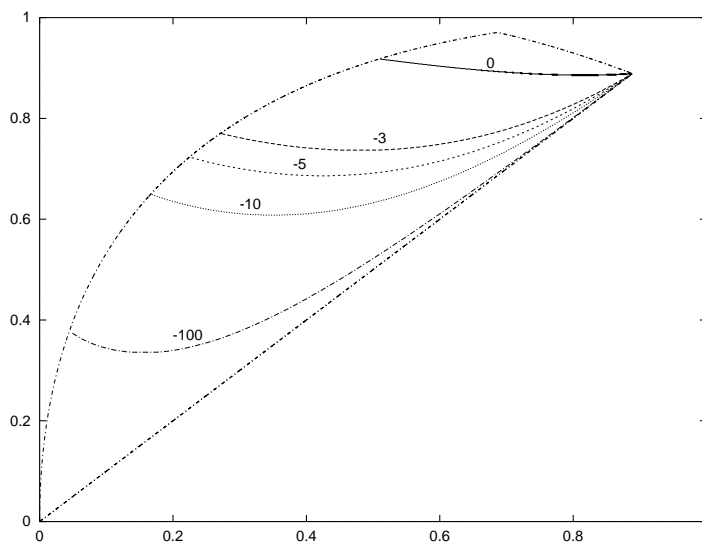


Figure 2: On each lines, $H(a_s, b_s; \beta) = 8/9$ for various values of β : 0, -3, -5, -10 and -100. Horizontal and vertical axes denote, respectively, b_s and a_s .

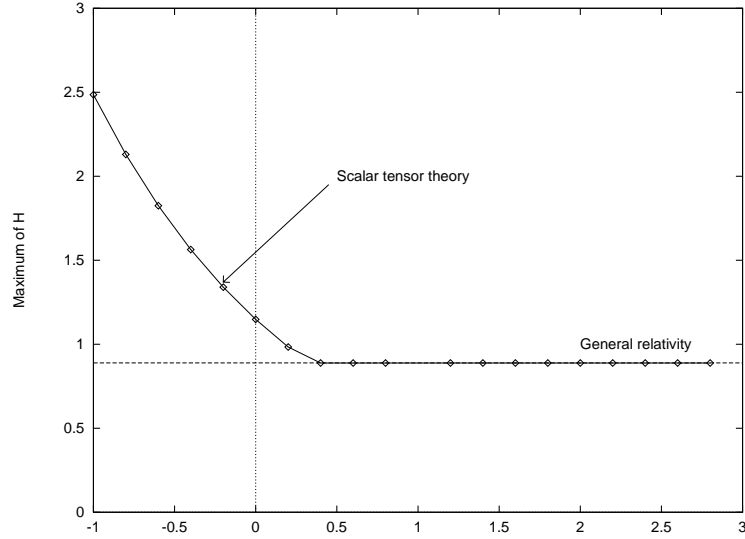


Figure 3: The Maximum mass-to-size ratio, H_{MAX} , is shown as a function of β . Horizontal and vertical axes denote, respectively, β , and H_{MAX} . A horizontal line, $H_{\text{MAX}} = 8/9$, denotes Buchdahl's limit in general relativity. When $\beta \lesssim 0.4$, H_{MAX} exceeds Buchdahl's limit. When $\beta \lesssim 0.2$, H_{MAX} exceeds unity, a black hole limit.

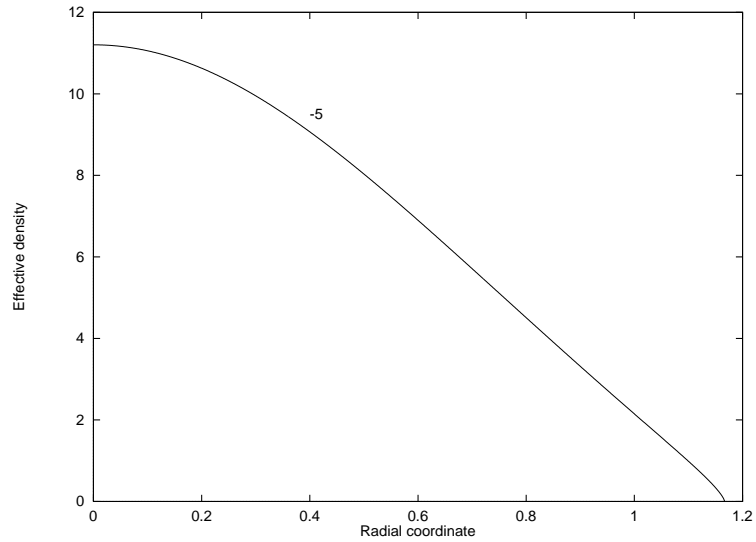


Figure 4: The effective density, $\rho_{\text{eff}}(r)$, is shown in the case that $\beta = -5$ and $n_c/n_0 = 10$. Horizontal and vertical axes denote, respectively, the radial coordinate, r , in the unit of 10km, and the effective density, $\rho_{\text{eff}}(r)/(m_b n_0)$. It is seen that the assumption, $\rho'_{\text{eff}}(r) \leq 0$, is satisfied.

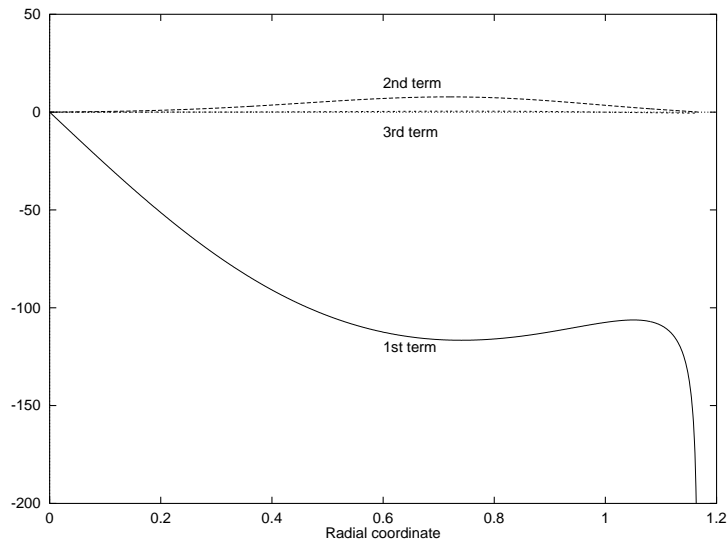


Figure 5: Each term of (4.5) in $\rho'_{\text{eff}}(r)$ is shown for $\beta = -5$ and $n_c/n_0 = 10$. Horizontal and vertical axes denote, respectively, the radial coordinate, r , in the unit of 10km, and the 1st, 2nd and 3rd terms in (4.5).

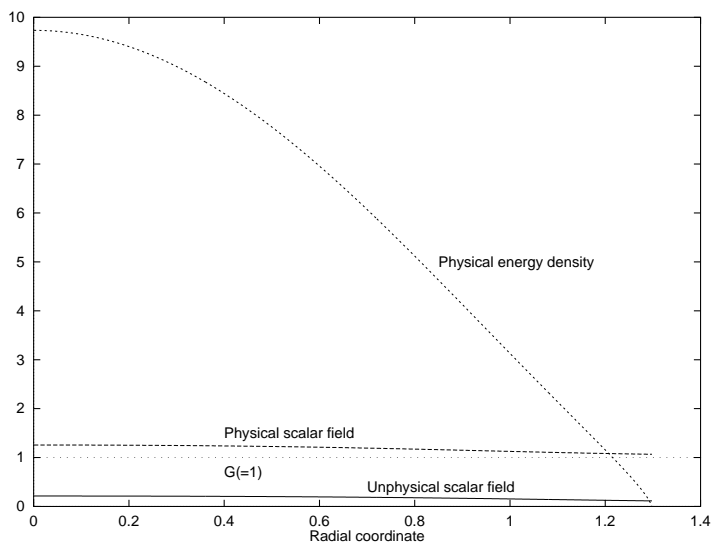


Figure 6: We compare $\phi(r)$, $\rho(r)$ and $\varphi(r)$ in the case that $\beta = -5$ and $n_c/n_0 = 7.9$. Horizontal and vertical axes denote, respectively, the radial coordinate, r , in the unit of 10km, and $\rho(r)/(m_b n_0)$, $\phi(r)$ and $\varphi(r)$. On a thin dotted line, $G \equiv 1/\phi_0 = 1$, i.e., general relativity.

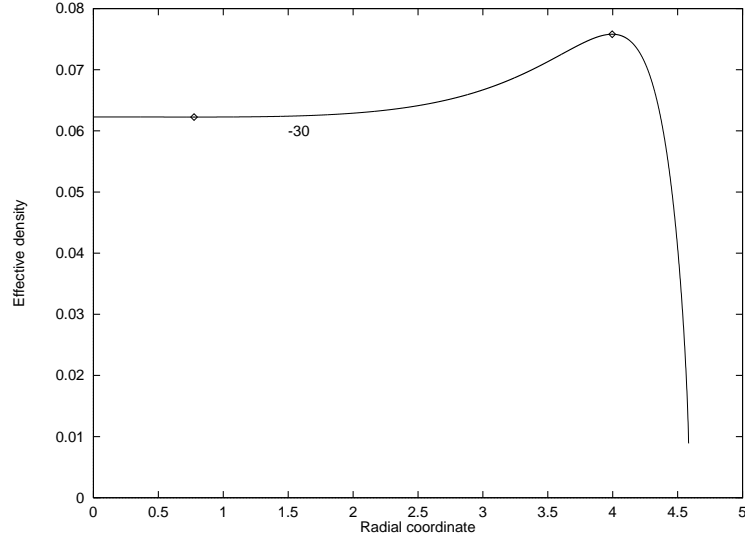


Figure 7: The effective density, $\rho_{\text{eff}}(r)$, is shown in the case that $\beta = -30$ and $n_c/n_0 = 10$. Horizontal and vertical axes denote, respectively, the radial coordinate, r , in the unit of 10km, and the effective density, $\rho_{\text{eff}}(r)/(m_b n_0)$. It is seen that the assumption, $\rho'_{\text{eff}}(r) \leq 0$, is partially violated between two rectangles.

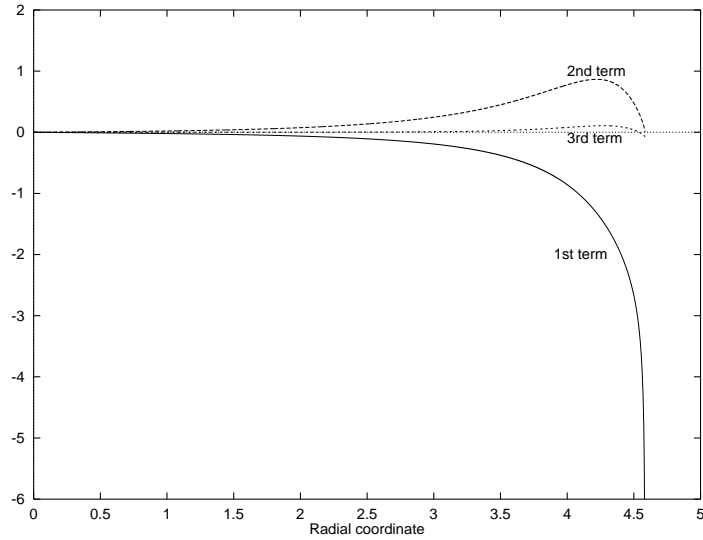


Figure 8: Each term of (4.5) in $\rho'_{\text{eff}}(r)$ is shown for $\beta = -30$ and $n_c/n_0 = 10$. Horizontal and vertical axes denote, respectively, the radial coordinate, r , in the unit of 10km, and the 1st, 2nd and 3rd terms in (4.5).

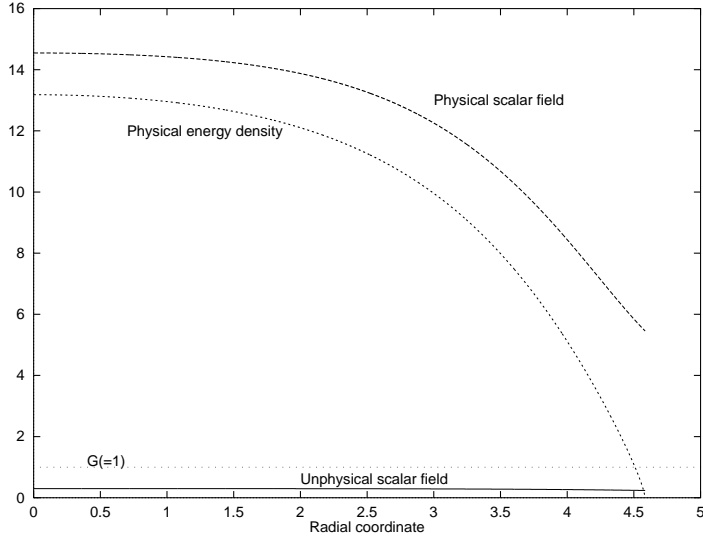


Figure 9: We compare $\phi(r)$, $\rho(r)$ and $\varphi(r)$ in the case that $\beta = -30$ and $n_c/n_0 = 10$. Horizontal and vertical axes denote, respectively, the radial coordinate, r , in the unit of 10km, and $\rho(r)/(m_b n_0)$, $\phi(r)$ and $\varphi(r)$. On a thin dotted line, $G \equiv 1/\phi_0 = 1$, i.e., general relativity.

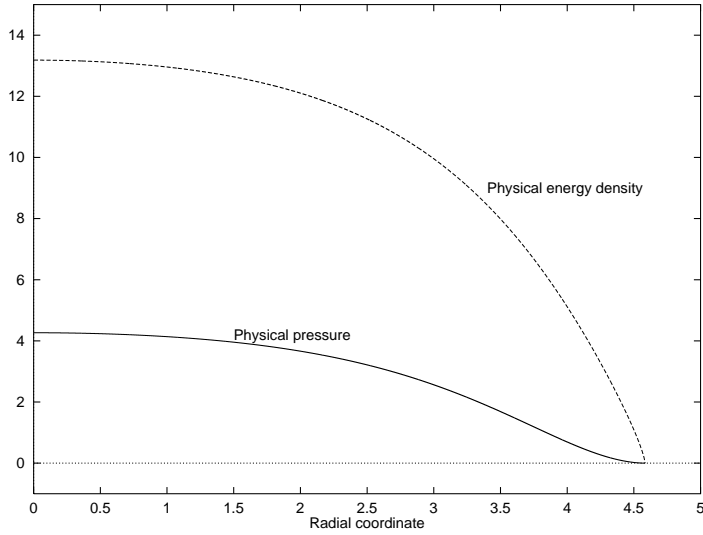


Figure 10: We show $\rho(r)$ and $p(r)$ in the physical frame for $\beta = -30$ and $n_c/n_0 = 10$. Horizontal and vertical axes denote, respectively, the radial coordinate, r , in the unit of 10km, and $\rho(r)/(m_b n_0)$ and $p(r)/(m_b n_0)$. Though the assumption, $\rho'_{\text{eff}}(r) \leq 0$, is violated in the Einstein frame, the conditions, $\rho(r) - 3p(r) \geq 0$, $\rho'(r) \leq 0$ and $p'(r) \leq 0$ are all satisfied in the physical frame.

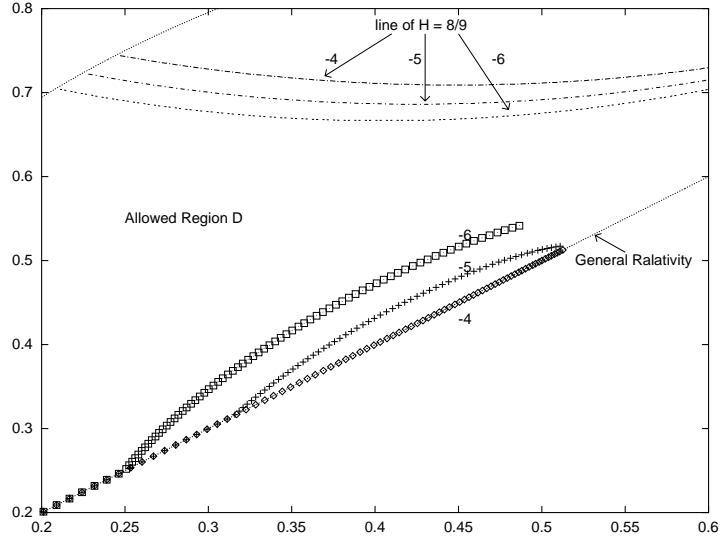


Figure 11: We show the parameters, (a_s, b_s) , in each equilibrium solution for $n_c/n_0 = 2.5 \sim 10.3$. We take $\beta = -4, -5$ and -6 , and impose the conditions, $\rho(r) - 3p(r) \geq 0$ and $\rho'_{\text{eff}}(r) \leq 0$. Horizontal and vertical axes denote, respectively, b_s and a_s .

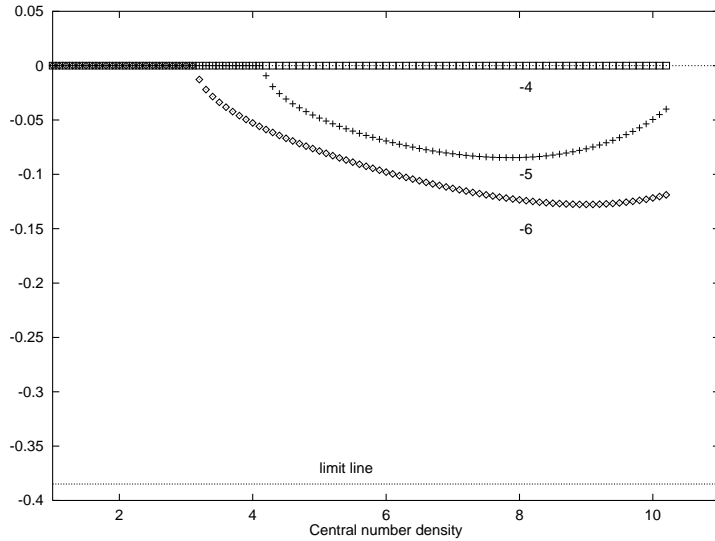


Figure 12: We show the parameter, c_s , in each equilibrium solution for $n_c/n_0 = 1.0 \sim 10.3$. We take $\beta = -4, -5$ and -6 , and impose the conditions, $\rho(r) - 3p(r) \geq 0$ and $\rho'_{\text{eff}}(r) \leq 0$. Horizontal and vertical axes denote, respectively, n_c/n_0 and c_s . A horizontal thin dotted line denotes the limit on c_s , i.e., $c_s = -2\sqrt{3}/9$.

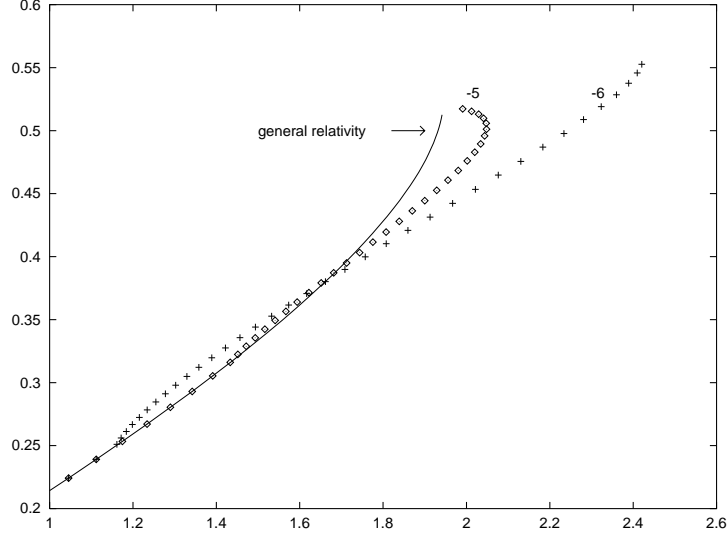


Figure 13: We show the relation between the mass-to-size ratio and the mass. We take $\beta = -5$ and -6 , and impose the conditions, $\rho(r) - 3p(r) \geq 0$ and $\rho'_{\text{eff}}(r) \leq 0$. Horizontal and vertical axes denote, respectively, M/M_{\odot} , and $2M/R$. The solid line represents the mass-to-size ratio in general relativity.

β	n_c/n_0	$\rho'_{\text{eff}} \leq 0$	$\rho - 3p \geq 0$	H_{max}
-12.07	0.1 ~ 10.3	○	○	0.679
	10.3 ~ 11.2	○	×	1.018
-11.0	0.1 ~ 10.3	○	○	0.666
	10.3 ~ 11.3	○	×	0.919
-10.0	0.1 ~ 10.3	○	○	0.651
	10.3 ~ 11.4	○	×	0.834
-6.0	0.1 ~ 10.3	○	○	0.556
	10.3 ~ 11.2	○	×	0.569
-5.0	0.1 ~ 10.3	○	○	0.517
	10.3 ~ 15.7	○	×	0.567
-4.0	0.1 ~ 10.3	○	○	0.514
	10.3 ~ 14.9	○	×	0.562
0.0	0.1 ~ 10.3	○	○	0.514
	10.3 ~ 14.9	○	×	0.562

Table 1: We summarize our numerical results. In the 1st column, β is given. In the 2nd column, we give a range of n_c from our numerical studies. In the 3rd and 4th columns, we indicate, respectively, whether the assumption, $\rho'_{\text{eff}} \leq 0$, and the condition, $\rho - 3p \geq 0$, are satisfied. In the 5th column, the maximum mass-to-size ratio is shown for each β .